PARTICLE DEPOSITION ON AN ARRAY OF SPHERES USING RANS-RSM COUPLED TO A LAGRANGIAN RANDOM WALK

A. Dehbi*, S. Martin†

** Laboratory for Thermal-Hydraulics, Paul Scherrer Institut, Villigen 5232, Switzerland*

† Laboratoire de Mécanique des Fluides et d'Acoustique, Ecole Centrale de Lyon, 69130 Ecully, France

Abstract

The Generation IV Pebble Bed Modular Reactor (PBMR) is being considered as a promising concept to produce electricity or process heat with high efficiencies and unique safety features. The PBMR is a high-temperature, helium-cooled, graphite moderated reactor. The fuel elements consist of 6 cm diameter spherical graphite "pebbles" containing each thousands of uranium dioxide microspheres.
As the pebbles continually rub against one another in the core, a significant quantity of graphite dust can be released in the reactor coolant system. These dust particles, which contain some amounts of fission products, are transported and deposited on pebbles as well as primary circuit surfaces. It is therefore of great safety interest to develop and benchmark numerical approaches for predicting deposition of dust particles in the various locations of the PBMR primary circuit.

In this investigation, we address turbulent particle deposition on the pebbles using the ANSYS-Fluent CFD code. We simulate particulate flows around linear arrays of spheres and compare deposition rates against experiments. It is found that the Reynolds Stress Model (RSM) combined with the Continuous Random Walk (CRW) to supply fluctuating velocity components predicts deposition rates that are generally within the scatter of the data.

1. INTRODUCTION

The Generation IV Pebble Bed Modular Reactor (PBMR) (Koster et al., 2003) is being considered as a promising concept to produce electricity or process heat with high efficiencies and unique safety features. The PBMR is a high-temperature, helium-cooled, graphite moderated reactor. The fuel elements consist of 6 cm diameter spherical graphite "pebbles" containing each thousands of uranium dioxide microspheres. As the pebbles are continually rubbing against one another in the core, a significant quantity of graphite dust can be released in the reactor coolant system. For example, the AVR reactor produced around 3-5 kg of graphite dust per year (Bäumer, 1990). These dust particles, which are a few microns in size, contain some amounts of fission products that are transported and deposited on pebbles as well as primary circuit surfaces. It is therefore of great safety interest to develop and benchmark numerical approaches for predicting deposition of dust particles in the various locations of the PBMR primary circuit.

In this investigation, we concentrate on turbulent particle deposition on the pebbles using the ANSYS Fluent Computation Fluid Dynamics (CFD) code. Validation of the flow field is first performed on a single sphere, which has been extensively studied both experimentally and computationally. We simulate thereafter particle motion on a single sphere, then on different sets of linear arrays of 8 spheres that have a range of spacings between 1.5 D and 6 D, D being the sphere diameter. We subsequently compare the particle deposition to the experiments performed by Hähner et al. (1994) and Waldenmaier (1999) over a range of sphere diameters and particle sizes.

Particulate transport in turbulent flows is traditionally simulated using two families of methods, namely the Eulerian and Lagrangian approaches. We choose here the Lagrangian approach (Maxey, 1987) which treats particles as a discrete phase dispersed in the continuum. The particle motion is naturally deduced from Newton's second law, allowing one to include all the relevant forces that are significant (drag, gravity, lift, thermophoretic force, etc.). Although computationally intensive because it involves tracking a large number of particles, the Lagrangian particle tracking (LPT) approach is easier to implement and interpret. We assume in addition that the dispersed phase is dilute enough not to affect the continuous flow field (one-way coupling).

In laminar flows LPT involves very few assumptions and approximations, and is hence able to accurately predict particle dispersion in quite complicated geometries. When turbulence is present in the flow, the computation of particle dispersion becomes significantly more involved because of the random velocity fluctuations that preclude the deterministic computation of particle trajectories. One can either compute particle trajectories simultaneously with the fluid field within a Large Eddy Simulation (LES) approach, but this entails very large CPU requirements. An alternative method is to specify the fluctuating velocity field within a RANS approach, and hence resort to stochastic computations of a great many trajectories with the aim to capture "average" particle dispersion, and this approach is employed here. Models based on the discrete random walk (DRW) have been used with success (Kallio and Reeks, 1989) to analyze particle transport in idealized inhomogeneous flows. A more general and promising approach is the so-called Continuous Random Walk (CRW) based on the non-dimensional Langevin equation (Illiopoulous et al., 2003). This method is in principle applicable to general inhomogeneous flows provided the underlying flow first and second moments are known with reasonable accuracy. The CRW describing the model for fluid velocity history is introduced next.

2. LAGRANGIAN PARTICLE TRACKING: RANS MODELLING

2.1 The particle equation of motion

We consider a rigid point-wise particle which is entrained in a turbulent flow at isothermal conditions. The only forces acting on the particle are taken to be drag and gravity. Brownian diffusion is ignored

as particles in this study have diameters greater than 1 μm. The lift force is also neglected as the particles are of the same unit density as the carrier fluid. The vector force balance on a spherical particle reduces then to:

$$\frac{dU_p}{dt} = F_D(U - U_p) + g = \frac{18\mu}{\rho_p d_p^2} C_D \frac{\mathrm{Re}_p}{24}(U - U_p) + g \quad (1)$$

where U is the fluid velocity, U_p the particle velocity, ρ_p the particle density, d_p the particle geometric diameter,. μ the fluid molecular viscosity, g the gravity acceleration vector, and Re_p the particle Reynolds number defined as:

$$\mathrm{Re}_p = \frac{d_p |U - U_p|}{\nu} \quad (2)$$

ν being the fluid kinematic viscosity. The drag coefficient is computed in the ANSYS-Fluent code (2008) from the following equation:

$$C_D = \beta_1 + \frac{\beta_2}{\mathrm{Re}_p} + \frac{\beta_3}{\mathrm{Re}_p^2} \quad (3)$$

where the β's are constants which apply to spherical particles for wide ranges of Re_p.

Since the carrier flow is quite turbulent, the mean flow velocity alone will not give satisfactory as particle deposition will not be predicted past the first sphere. Therefore turbulent fluid fluctuations have to be modeled.

The fluid velocity see by particles can hence be decomposed as follows:

$$U = \overline{U} + u \quad (4)$$

$\overline{U}$ Is considered the time-averaged fluid provided by the RANS approach and *u* is the fluctuation part. Various models have been proposed to specify u, the most promising of which is the stochastic Langevin model which is particularly suited for inhomogeneous flows.

The stochastic Langevin equations defining the fluctuating velocity field along a particle track are presented briefly. The domain is subdivided in two regions: the boundary layer region with strongly anisotropic turbulence, and a bulk region with generally anisotropic and inhomogeneous turbulence. The Langevin equations will take different forms depending on the location of the particle.

2.2 The Langevin model for turbulent fluid fluctuations

2.2.1 The Langevin equation in boundary layers

Following Iliopoulos et al. (2003), the normalized Langevin equation for the fluid velocity fluctuation along the i^{th} coordinate is written as:

$$d(\frac{u_i}{\sigma_i}) = -\left(\frac{u_i}{\sigma_i}\right)\cdot\frac{dt}{\tau_L} + d\eta_i + A_i dt \tag{5}$$

In the above, u_i is the fluid fluctuating velocity component, σ_i the rms of velocity $\sqrt{\overline{u_i^2}}$, τ_L a Lagrangian time scale, $d\eta_i$ a succession of uncorrelated random forcing terms, and A_i the mean drift correction term which ensures the well-mixed criterion (Thomson, 1987). For particles with general inertia, A_i can be written as follows (Bocksell and Loth, 2006):

$$A_i = \frac{\partial(\frac{\overline{u_i u_j}}{\sigma_i})}{\partial x_j}\cdot\frac{1}{1+\tau_p^+} \tag{6}$$

The dimensionless relaxation time number τ_p^+ is defined as:

$$\tau_p^+ = \frac{\tau_p}{\tau_L} \tag{7}$$

In the above, τ_L is a Lagrangian time scale to be specified later, and τ_p the particle relaxation time defined according to the prevailing particle Reynolds number. Dehbi (2008) has shown that the normalized Langevin equations can be simplified in the boundary layer and cast as follows for the body-fitted streamwise, normal, and spanwise directions of the boundary layer ($y^+ > 100$):

$$d(\frac{u_1}{\sigma_1}) = -(\frac{u_1}{\sigma_1})\cdot\frac{dt}{\tau_L} + \sqrt{\frac{2}{\tau_L}}\cdot d\xi_1 + \frac{\partial\left(\frac{\overline{u_1 u_2}}{\sigma_1}\right)}{\partial x_2}\cdot dt \tag{8}$$

$$d(\frac{u_2}{\sigma_2}) = -(\frac{u_2}{\sigma_2})\cdot\frac{dt}{\tau_L} + \sqrt{\frac{2}{\tau_L}}\cdot d\xi_2 + \frac{\partial\sigma_2}{\partial x_2}\cdot dt \tag{9}$$

$$d(\frac{u_3}{\sigma_3}) = -(\frac{u_3}{\sigma_3})\cdot\frac{dt}{\tau_L} + \sqrt{\frac{2}{\tau_L}}\cdot d\xi_3 \tag{10}$$

where the $d\xi_i$'s are taken to be an uncorrelated succession of Gaussian random numbers with zero mean and variance dt.

2.2.2 The Langevin equation in boundary layers

In the bulk region, for which $y^+ \geq 100$, turbulence can be expected to be both anisotropic and inhomogeneous given the complex flows of this investigation. No simplifications of the drift coefficient can be made, since one is away from the boundary layer, and hence the Langevin equations for the bulk region can then be expressed in the computational domain as follows:

$$d(\frac{u_1}{\sigma_1}) = -(\frac{u_1}{\sigma_1})\cdot\frac{dt}{\tau_L} + \sqrt{\frac{2}{\tau_L}}\cdot d\xi_1 + A_1\cdot dt \tag{11}$$

$$d(\frac{u_2}{\sigma_2}) = -(\frac{u_2}{\sigma_2})\cdot\frac{dt}{\tau_L} + \sqrt{\frac{2}{\tau_L}}\cdot d\xi_2 + A_2\cdot dt \tag{12}$$

$$d(\frac{u_3}{\sigma_2}) = -(\frac{u_3}{\sigma_2}) \cdot \frac{dt}{\tau_L} + \sqrt{\frac{2}{\tau_L}} \cdot d\xi_3 + A_3 \cdot dt \qquad (13)$$

The drift terms A_i as used as defined by equation (6) without further approximation. The necessary Reynolds stress values are given by the RSM model.

2.3 Required Eulerian statistics

The flow in the boundary layer is modeled in the RANS framework, and the prevailing Eulerian statistics are assumed to be reasonably well approximated by those given by Direct Numerical Simulation (DNS) investigations of fully developed channel flows. This approximation yielded reasonable estimations of the particle deposition rates in a variety of geometries (Dehbi, 2008), and is deemed better than using directly the RSM statistics, because the latter are known to be inaccurate very near the wall. The channel flow DNS data by Marchioli et al. (2006) were curve-fitted to give the rms of velocity by ratios of polynomials of order 3 to 5 and match the data with a correlation coefficient better than 0.99:

$$\sigma_i^+ \equiv \frac{\sigma_i}{u^*} = \frac{\sum_j a_j y^{+j}}{\sum_k b_k y^{+k}} \qquad (14)$$

y^+ is the wall distance in dimensionless units defined as:

$$y^+ = \frac{y u^*}{\nu} \qquad (15)$$

y is the particle distance to the nearest wall, u* the friction velocity derived from the wall shear stress τ_w and wall fluid density ρ_f as follows:

$$u^* = \sqrt{\frac{\tau_w}{\rho_f}} \qquad (16)$$

The cross-term $\overline{u_1 u_2}/\sigma_1$ in equation 7 was curve-fitted in similar fashion.

For the estimation of the fluid Lagrangian time scale τ_L, Bocksell and Loth (2006) have performed DNS calculations in the boundary layer and showed that the Lagrangian time scales in all directions are nearly equal and quite well approximated by the fits obtained by Kallio and Reeks (1989) and given by:

$$\tau_L^+ = 10 \qquad y^+ \leq 5 \qquad (17)$$

$$\tau_L^+ = 7.122 + 0.5731 \cdot y^+ - 0.00129 \cdot y^{+2}, \quad 5 < y^+ < 100$$

Where:

$$\tau_L^+ = \frac{\tau_L \cdot u^{*2}}{\nu} \qquad (17)$$

The Lagrangian time scale in the bulk is calculated from the total turbulent kinetic energy *k* and dissipation rate ε as follows:

$$\tau_L = \frac{2}{C_o} \cdot \frac{k}{\varepsilon} \tag{18}$$

A value of 14 for C_o provides good agreement with time scales computed DNS investigations (Mito and Hanratty, 2002).

2.4 Coupling the CRW model to the ANSYS-Fluent code

The ANSYS-Fluent CFD code (ANSYS, 2008) provides the mean flow parameters as well as a module to integrate the particle equations of motion. The Langevin model described earlier was implemented in ANSYS-Fluent as a User Defined Function (UDF) subroutine which supplies the trajectory calculation module with the fluctuating fluid velocity seen by a particle at each time step. Details of the coupling between the ANSYS-Fluent CFD code and the stochastic Langevin model are provided by Dehbi (2008).

3. RESULTS

3.1 General background

Many investigations of flows past a sphere have been conduced both experimentally and numerically. In order to characterize these flows, dimensionless number are used, the more common ones being the friction coefficient C_f, the pressure coefficient C_p and the drag coefficient C_D. The former two are defined on a local point on a sphere surface, whereas the latter is an integral value over the whole sphere surface. Mathematically, the coefficients are defined as:

$$C_p = \frac{P - P_\infty}{\frac{1}{2}\rho_f u_\infty} \tag{19}$$

$$C_f = \frac{\tau_w}{\frac{1}{2}\rho_f u_\infty \cdot \mathrm{Re}^{1/2}} \tag{20}$$

$$C_D = \frac{F_D}{\frac{1}{2}\rho_f u_\infty A} \tag{21}$$

where P is the wall pressure, P_∞ free stream pressure, u_∞ the free stream velocity, τ_w the wall shear stress, ρ_f the fluid density, and F_D the total drag force, A the projected sphere area, and Re the Reynolds number based on the sphere diameter. The drag coefficient versus Reynolds number as determined from experiments is show in Figure 1.

For Re <1 the flow is laminar and symmetric (Stokes flow) and the drag coefficient can be shown analytically to be 24/Re. For 1<Re<1000, the drag coefficient continues to decrease but at a slower rate. For 10^3< Re < $2.5*10^5$ the drag reaches a plateau and stays constant at an empirically determined value is around 0.4. It is this subcritical range which is of interest in this investigation. At around Re ≈ $2.5*10^5$, the drag coefficient abruptly decreases from 0.4 to less than 0.1 as the boundary layer becomes fully turbulent and separation is significantly reduced.

One of the most often cited experimental data used is that Achenbach (1970) who gives the values of pressure and friction coefficients on the surface of the sphere for a sub-critical value of Re (Figure 1).

A more recent study made by Jang et al.(2008) gives visualization of the flow structure around a sphere for Re = 11,000.

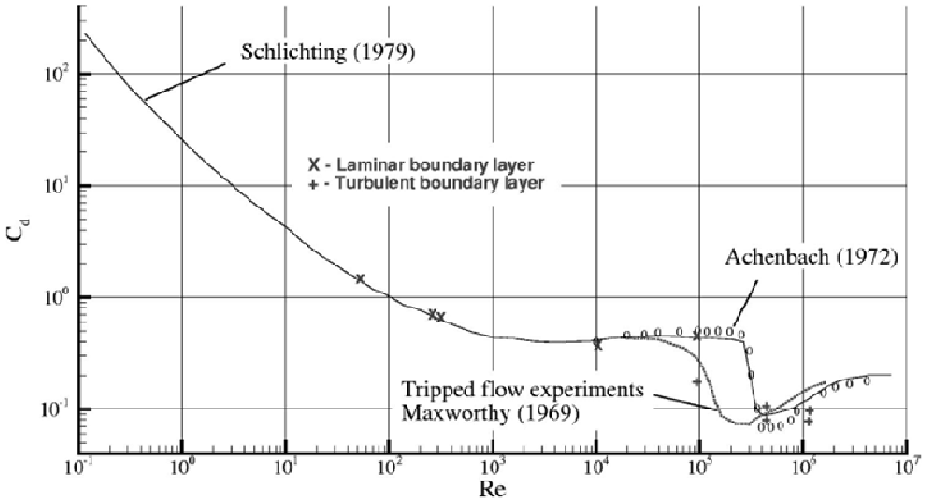

Figure 1: Drag coefficient for uniform flow past a sphere

Numerical investigations have also been conducted on flow past a sphere in order to benchmark turbulence models. For example Constantinescu et al. (2003, 2004) made 3D computations using unsteady RANS equations with several turbulence models like k-ε and k-ω. They also made computations using LES and DES. Their results show that URANS predictions of the pressure coefficient, skin friction and streamwise drag were in reasonable agreement with measurements, and predictions of turbulence kinetic energy and the shear stress were similar to LES and DES results. However URANS solutions did not adequately resolve shedding mechanisms while LES and DES managed to resolve a large part of the vortex shedding process.

3.2 Meshing, grid-independence and turbulence modeling

The particulate flow experiments that are simulated in this investigation involve single spheres as well as well as linear arrays of 8 spheres with diameters in the range of 3.2 mm to 9 mm and different inter-sphere spacings L/D of 1.5, 2 and 6. The spheres are positioned in the center of a pipe with diameter 100 mm (Figure 2). A distance of 7 sphere diameters is allowed upstream of the front sphere such that flow and particles reach developed conditions. Owing to the symmetric nature of the problem, only one quarter of the geometry is meshed, hence significantly reducing the number of meshes required.

Structured hexahedral meshes are used to discretize the domain. The boundary layer is fully resolved, and in compliance with the best practice guidelines (2000), the following criteria are adopted: a) the wall nearest cell centroid has a y+ of order 1; b) the laminar and buffer layer (up to y+ of 30) has 5 to 10 grid points; and c) the entire boundary layer has 20 to 30 grid points. The grading factor is typically about 1.1, which gives a mesh as shown in Figure 3. Once the single sphere mesh is constructed, the meshes for linear arrays are obtained by simply copying the single sphere mesh as many times are required. The Reynolds stress model (RSM) of turbulence is used for all the simulations as it considered the most physically sound RANS model. Third order MUSCL scheme is used for the discretization of the RANS equations.

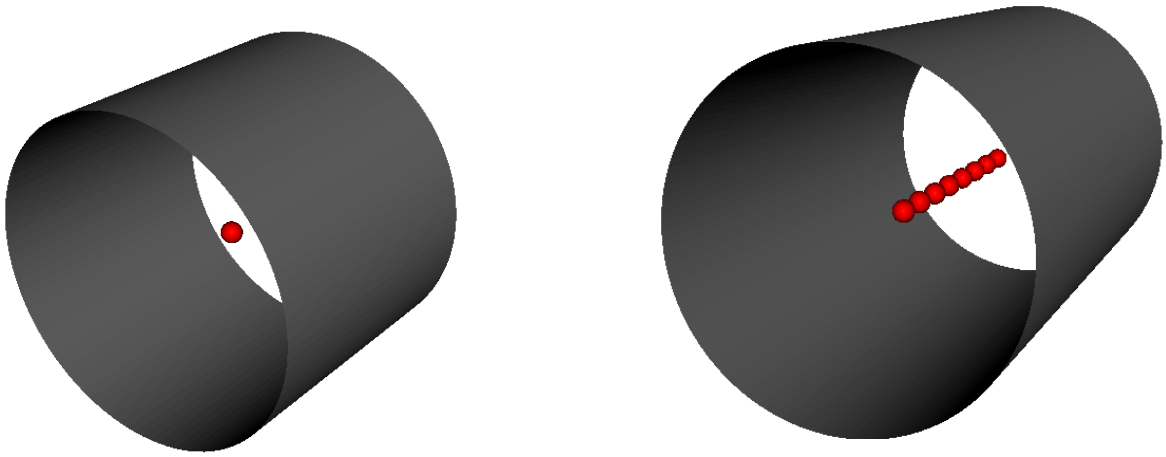

Figure 2: Examples of global geometries

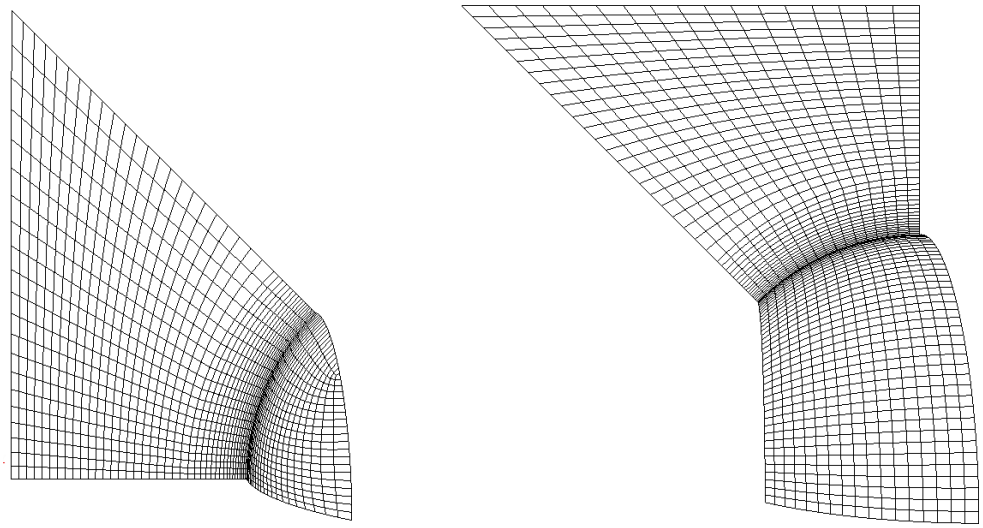

Figure 3: Grading in the boundary layer

For each simulation, a hierarchy of grids is constructed with coarse, medium and fine grid resolution. Grid sensitive quantities such as the drag and lift coefficient are checked to ensure that the results are grid-independent. The results of a sample grid-independence study for an array of 8 spheres with L/D = 2 and Re of 12000 is presented. Table 1 shows mean values of global parameters for the lead sphere. Figure 4 shows profiles of selected variables. The profiles are extracted from the 4^{th} sphere surface (Pressure and shear stress) and along its wake (velocity and turbulent kinetic energy). As can be seen, the results can be considered grid independent.

Grid	Cells Count (millions)	Lead Sphere		
		Mean y+ wall	Drag Coefficient	Viscous Drag (%)
Coarse	1.1	1.29	0.393	9.3
Medium	1.6	1.29	0.394	9.3
Fine	2.4	1.29	0.395	9.3

Table 1 : Grid sensitivity for an array of 8 spheres at Re = 12000;

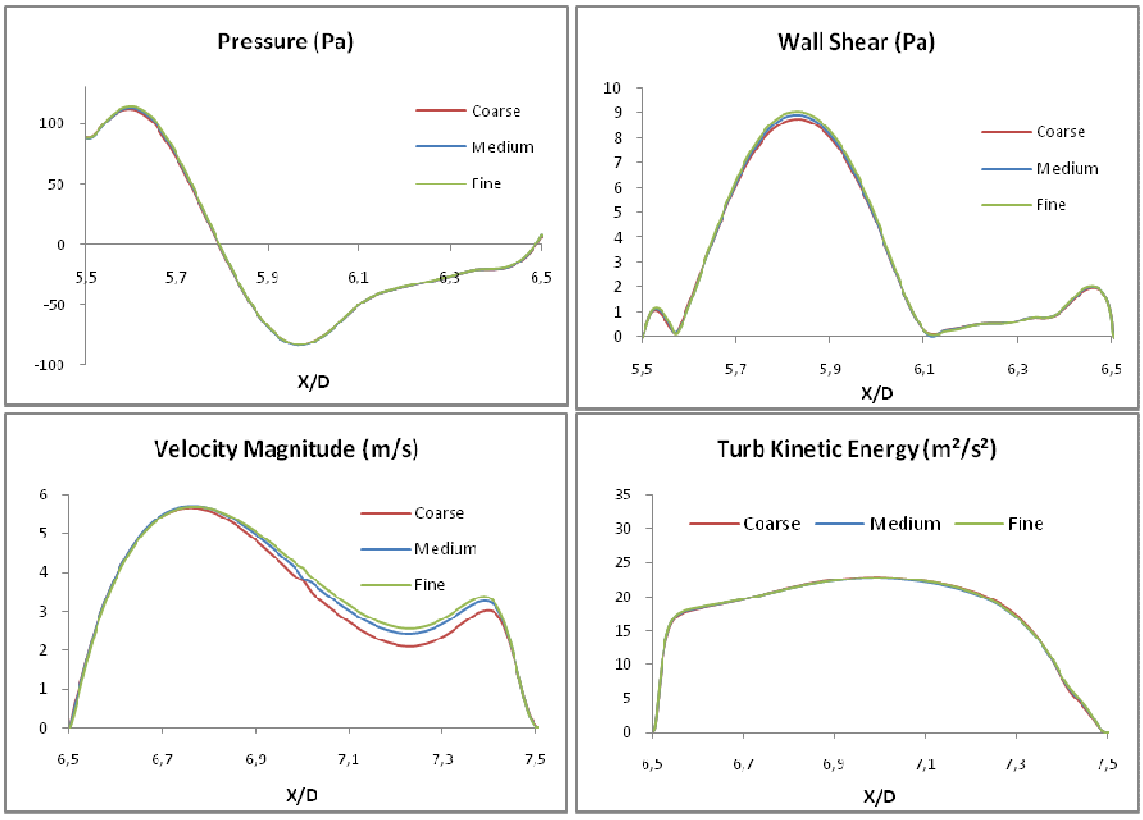

Figure 4: Grid sensitivity for an array of 8 spheres at Re = 12000;

3.3 Flow field validation for a single sphere

The simulation predicts a mean drag coefficient on a single sphere at Re=12000 of 0.47, somewhat above the range of the experimentally measured values C_D = 0.39 – 0.41 in Achenbach's experiments (1970), which is reasonably accurate. The pressure and friction factor angular distributions along the sphere surface are also compared in Figure 5. The predictions are globally in good agreement with the data. The laminar boundary layer separation is predicted to occur at an angle of 94°, which is somewhat higher than the measured value of 82.5°. The RANS investigations by Constantinescu et al. (2003, 2004) have used k-ε, k-ω, and v2f models, rather than RSM used here. Although some predictions obtained there are in better agreement with the data, the differences with our investigation are small.

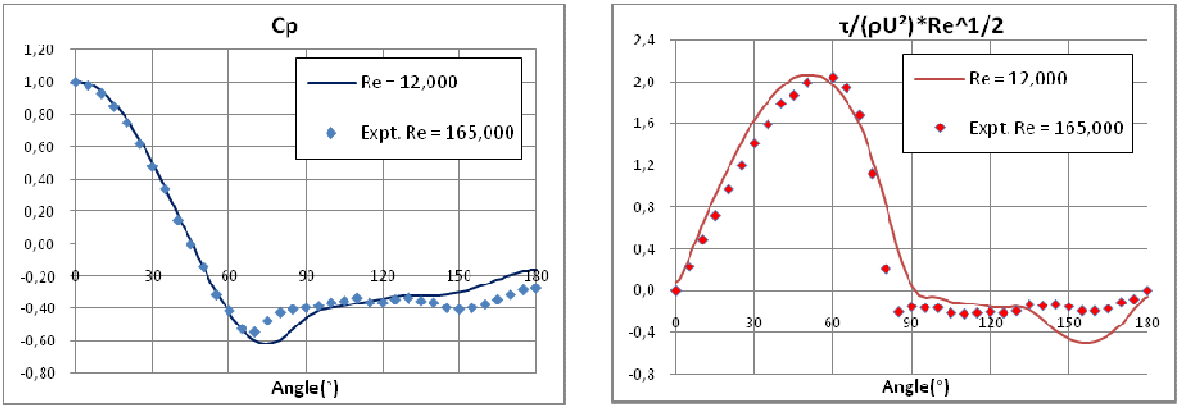

Figure 5: Comparison with data for a single sphere at Re = 12000

It is to be noted, however, that the wake area is not well predicted by the RSM when compared to the PIV of results obtained by Jang et al. (2008) at similar Reynolds number (Re=11000). As seen in Figure 6, the predicted wake recirculation area extends to 1 diameter beyond the sphere, whereas the PIV shows that it extends only to ½ diameter. This means that the particle tracking for regions beyond the lead sphere are expected to be affected by the inaccuracies in flow prediction in the wake area.

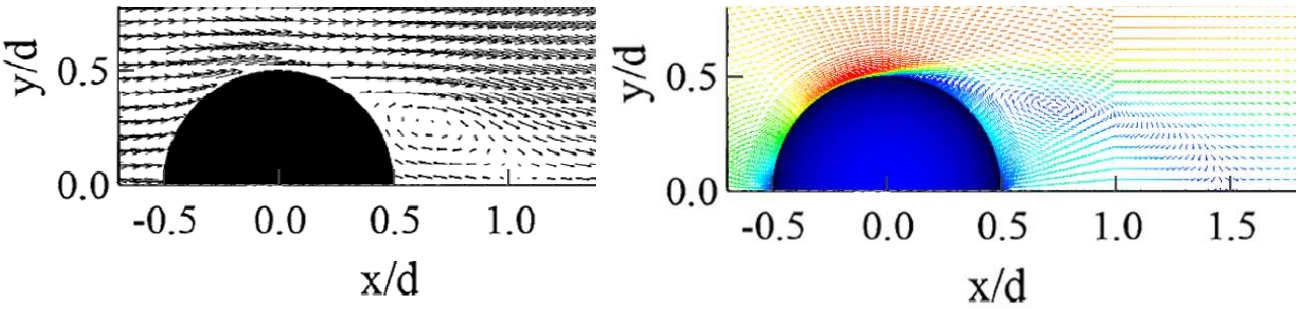

Figure 6: Comparison of PIV (left) and RANS (right) flow fields for a single sphere

3.4 Particles deposition on a single sphere: comparison with data

The majority of experimental work on particle deposition onto spheres has concentrated on single spheres. However, in practical applications, if the spheres are close to one another, the deposition on one sphere can be greatly influenced by the presence of neighboring spheres, as the interaction of wakes renders the fluid problem quite a bit more complex than that prevailing for single, isolated spheres.

A few experiments have been conducted on particles deposition on spheres. Noteworthy among these are the works of Hähner et al. (1994) and Waldenmaier (1999). In these two investigations, the same experimental setups were used. Air in a 100 mm pipe carries particles made of DEHS (density 915 kg/m^3) over single spheres or linear arrays of steel spheres varying in diameter between 3 and 9 mm. The spheres are mounted on thin wires which are fixed to the pipe by frames. The bulk air velocity is varied between 5 and 28 m/s, and the Reynolds number based on the sphere diameter ranges from 3000 to 12000. Monodisperse particles are produced via a condensation aerosol generator, and the spherical particles have geometric diameters between 1.5 and 15 μm.

The deposited mass on the spheres is determined using a washing technique combined with gas chromatographic detection methods. The collection efficiency is computed using the expression:

$$\eta = \frac{M_{deposited}}{C_{bulk} \cdot A \cdot Q} \tag{20}$$

where $M_{deposited}$ is the mass deposited on the sphere, C_{bulk} the bulk particle mass concentration upstream of the first sphere, A the projected area of the sphere, and Q the volumetric flow rate in the pipe.

The DEHS is a sticky liquid with very low vapor pressure, and bounce was confirmed to be negligible. The particle Stokes number was varied between 0.03 and 5, where the Stokes number is defined as the ratio of the particle relaxation time to a typical fluid flow time:

$$St = \frac{\tau_p}{D/2u_\infty} = \frac{\rho_p d_p^2}{9\mu} \cdot \frac{u_\infty}{D} \tag{21}$$

Particle which strike the collector are assumed to be immediately absorbed, consistent with experimental evidence. It is also assumed that a particle is trapped if its center comes within a distance less than the particle radius.

Given that the stochastic particle tracking is a Monte Carlo process, the number of particles injected has to be large enough for the sample size not to affect the results. Ideally one would inject very large number of particles uniformly at the inlet of the pipe and subsequently track particles. However, given the large ratio of the diameters between the spheres and the pipe (15.4), this would be a waste of computing time as the particles far from the center of the pipe have a negligible chance to deposit on the spheres. The injection area must therefore be smaller than the area of the pipe. Experimentation showed that injecting particle from a surface area spanned by 3 D is enough not to affect the results (differences in deposition efficiency less than 1%). Subsequently, all particle tracking simulations where conducted with an injection surface having a diameter of 5 D. The total number of computed trajectories is therefore 25 times larger than the number of particles injected from the surface equivalent to the projected area of the sphere. The latter number was varied depending on cases (particle inertia) from 10000 up to 100000, until results became independent of sample sizes.

For a single sphere, the experimentalists fixed the size of the collector, and varied both the Reynolds and Stokes numbers. Preliminary simulations showed that for a fixed Stokes number, deposition is very weakly dependant on Reynolds numbers in the range of interest (3000-12000). It is therefore appropriate to fix the Reynolds numbers in the simulation to a mid-range value, and vary the Stokes number by simply varying the particle diameter. The simulation is therefore performed for a sphere of diameter 6.5 mm at Re= 6000.

The error on the data was not reported in the experiments; however, one can have an idea about the magnitude of the scatter by plotting all data points for the deposition efficiency on a single plot, as in Figure 7. An upper and lower bound were drawn, excluding the two outliers at very low Stokes number and smallest sphere diameter (3.2 mm). In addition, a best fit curve of deposition efficiency is also shown. It can be seen that scatter at Stokes number less than 0.1 is significant, and for that region, the ratio of deposition efficiencies between the minimum and maximum band is between 3 and 4. This ratio decreases steadily and reaches a plateau of about 1.50 at Stokes numbers greater or equal to 0.7. In light of this, the simulations shown in Figure 8 are in general good agreement with the data and within the uncertainly band for most of the range of Stokes numbers. It is worth noting that particles strike the surface of the sphere essentially by inertial impaction, turbulent diffusion having

little effect. This was verified by tuning off the turbulent dispersion model, and using only the mean flow field in the particle equation of motion. Turbulence effects will however be significant when dealing with arrays of spheres.

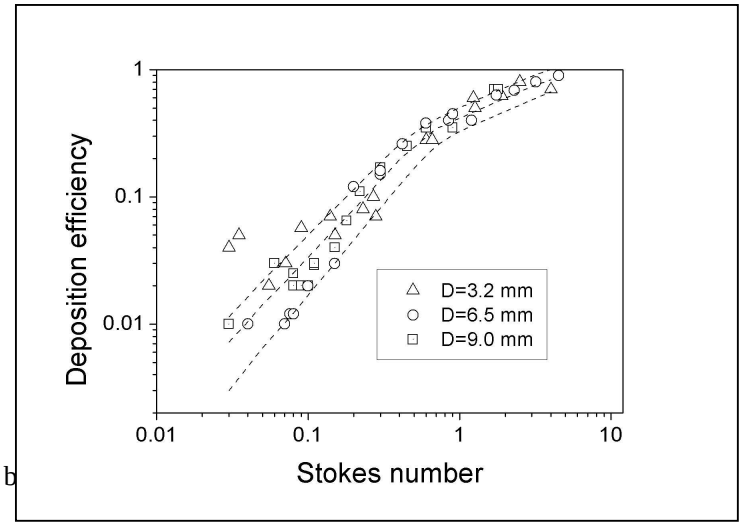

Figure 7: Scatter b

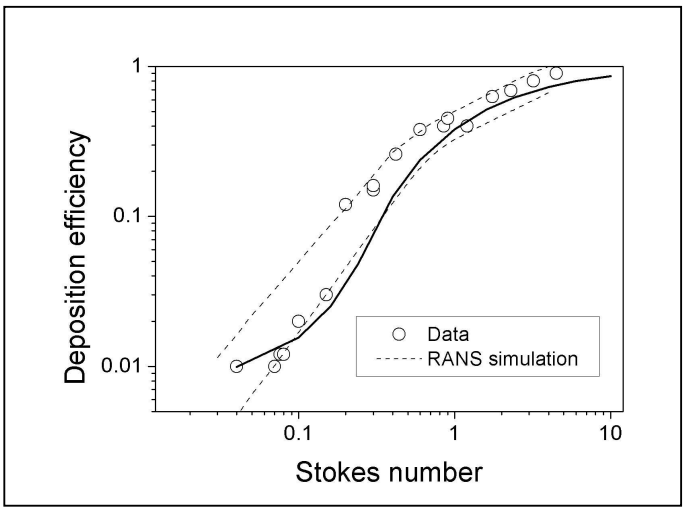

Figure 8: Comparison with data of particle deposition on a single sphere at Re= 6000 and D= 6.5 mm

3.5 Particles deposition on arrays of spheres: comparison with data

For arrays of spheres, 10 sets of experimental data were simulated. Conditions of the simulations are shown in Table 2, where X indicates that experimental data is available. Deposition rates are computed on the array of spheres in similar fashion to the procedure explained for a single sphere. Results of the simulations are shown in Figures 9 through 11 for L/D of 1.5, 2 and 6, respectively. On each plot, the particle deposition fraction is shown for sphere 1 (lead sphere) to sphere 8 (last sphere). The scatter of the data is given by the thick lines showing lower and upper bounds. The latter are deduced from the scatter in the single sphere experiments, i.e. for fixed mean deposition efficiency, minimum and maximum values are read from the plot displayed in Figure 7.

Re	Diameter	Stk	L/D

	(mm)		1.5	2	6
3000	3.2	0.3		X	X
6000	6.5	0.03		X	X
		0.04	X		
		1.2	X	X	X
		2.3	X		
8300	9	0.44	X		

Table 2: Particles tracking computations summary (X = data available)

Results show, as in the case of the single sphere, that the predictions are generally within the scatter band, except for very low deposition rates (Stokes number). For particles with medium and high inertia (Stokes number 0.3 and higher), the deposition trends are reproduced e.g. the "shielding effect" in which deposition on the lead sphere is significantly higher than that of the following spheres, the latter effect being less pronounced with a spacing of L/D=6.. At very low Stokes numbers (0.03-0.04), particles respond instantaneously to fluctuations of the fluid field, and effects such as "reverse shielding" (Waldenmaier, 1999). i.e. deposition on the second sphere larger than on the lead sphere, are not predicted. For these very small Stokes numbers, more fundamental turbulence models such as LES may be required to achieve better accuracy.

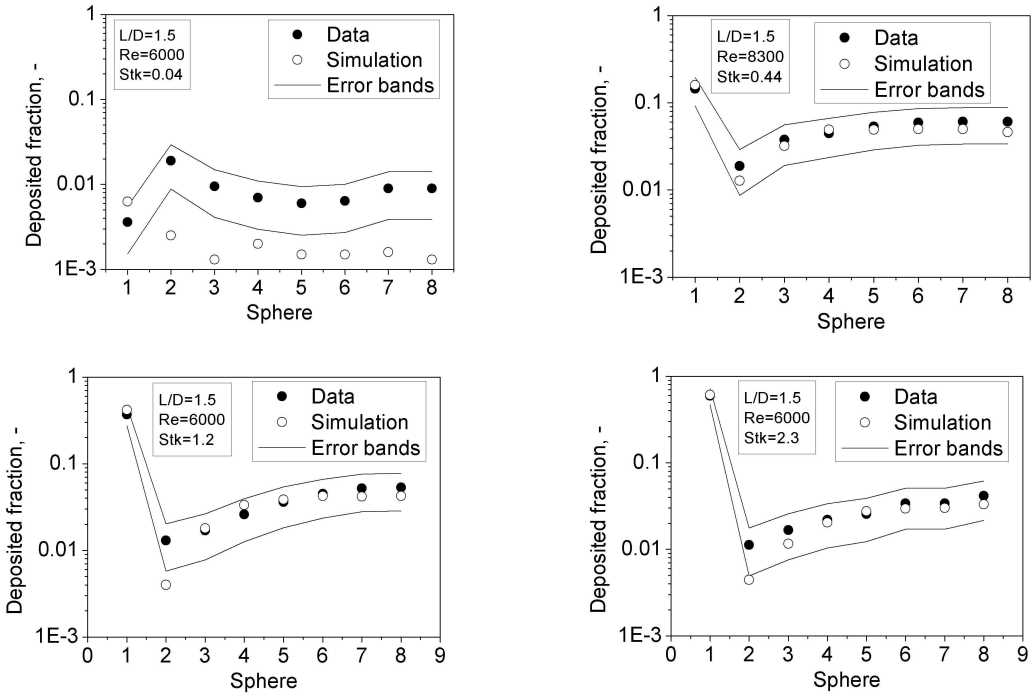

Figure 9: Comparison simulation and data for deposition on arrays of spheres. L/D=1.5

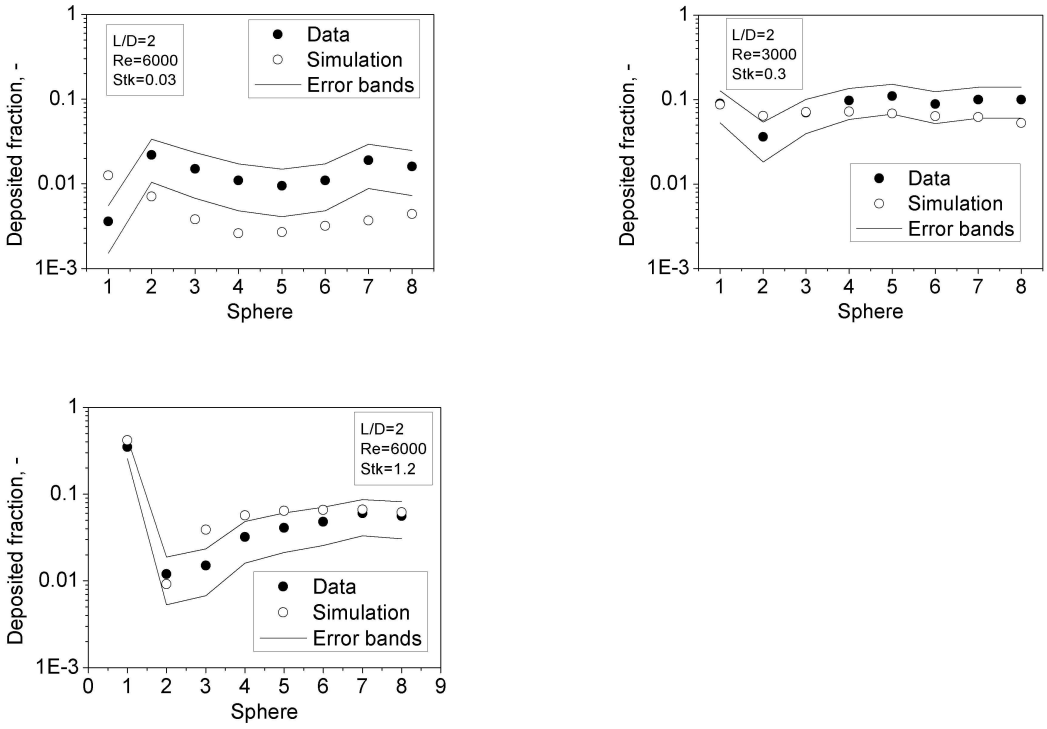

Figure 10: Comparison simulation and data for deposition on arrays of spheres. L/D=2

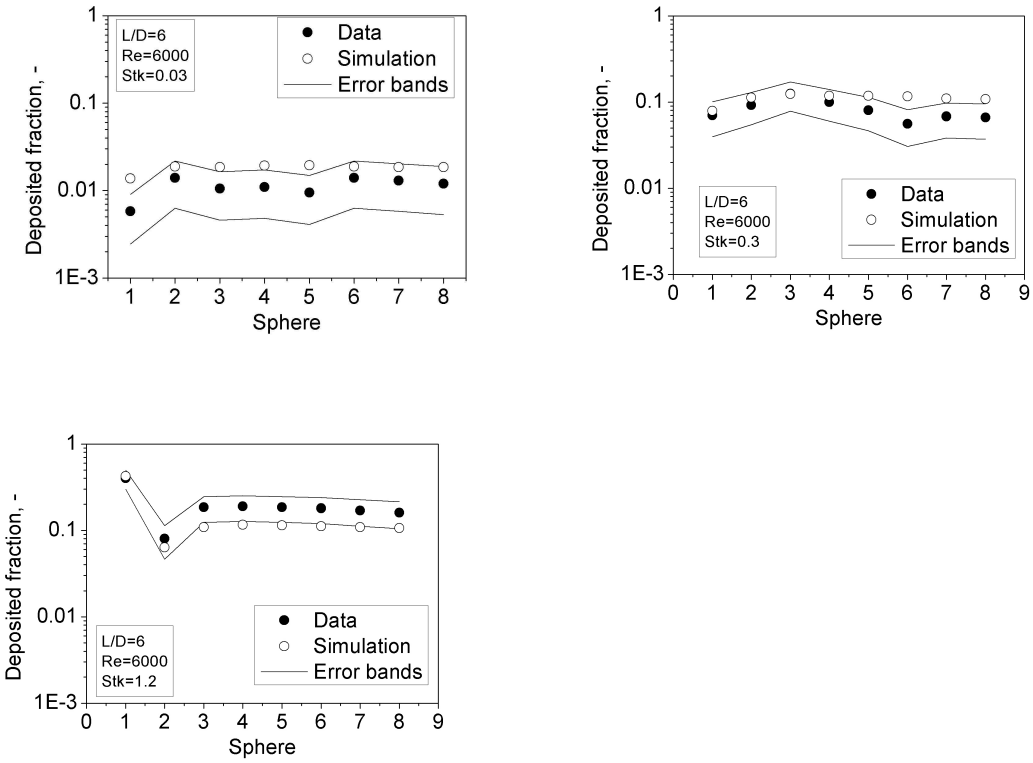

Figure 11: Comparison simulation and data for deposition on arrays of spheres. L/D=6

CONCLUSIONS

In this investigation, we focus on turbulent particle deposition on spheres using the ANSYS Fluent Computation Fluid Dynamics (CFD) code. We simulate flow and particle motion first on a single sphere, then on different sets of linear arrays of 8 spheres that have a range of inter-sphere spacings. The predicted particle deposition is compared to experiments performed by Hähner (1994) and Waldenmaier (1999) over a range of Reynolds numbers, sphere diameters and particle sizes. The Reynolds Stress Model (RSM) is used to compute the flow field and Best Practice Guidelines are followed to a large extent. The single sphere results for drag and shear stress distributions are compared to the experimental data of Achenbach (1970) and found to be in excellent agreement.

Lagrangian particle tracking is performed using the RSM mean flow field to which is added a fluctuating field computed by a continuous random walk (CRW) based on the non-dimensional Langevin equation.

Particle deposition on a single sphere is predicted with reasonable accurately by the RANS-CRW model. For an array of spheres, the accuracy of the prediction depends on the particle inertia: for very low inertia (Stokes number 0.03), the model predicts collection efficiencies that are low (order of 1%), in agreement with the data. However, qualitative effects such as the "reverse shielding" are not captured. For particles with mid and high inertia, the deposition trends are reproduced e.g. the "shielding effect" in which deposition on the lead sphere is significantly higher than that of the following spheres. The magnitudes of deposition efficiencies are generally predicted within the scatter of the experimental data.

REFERENCES

ANSYS Fluent 12 Users Guide, 2008.

E. Achenbach “Experiments on the flow past spheres at very high Reynolds numbers”, *Journal of Fluid Mechanics* 54, 565-575 (1970).

T.L. Bocksell, E. Loth, Stochastic modeling of particle diffusion in a turbulent boundary layer. *International Journal of Multiphase Flow* 32, 1234-1253 (2006).

R. Bäumer, “AVR – Experimental High-Temperature Reactor”, VDI-Verlag GmbH, Düsseldorf, Germany (1990).

G. Constantinescu, K. Squire, “Turbulent Modeling Applied to Flows over a Sphere”, *AIAA Journal*, 41, (2003).

G. Constantinescu, K. Squire, “Numerical investigations of flows over a sphere in the subcritical and supercritical regime”, *Physics of Fluids*, 16 (2004).

A. Dehbi, “Turbulent particle dispersion in arbitrary wall-bounded geometries: A coupled CFD Langevin-equation based approach”, *International Journal of Multiphase Flow* 34, 819-828 (2008).

ERCOFTAC. European Research Community on Flow Turbulence and Combustion (ERCOFTAC) Best Practice Guidelines, Version 1 (2000).

F. Hähner, G. Dau, F. Ebert “Inertial impaction of aerosol particles on single and multiple spherical targets”, *Chem. Eng. Technol.* 17, 88-94 (1994).

I. Iliopoulos I., Y. Mito, T.J. Hanratty, A stochastic model for solid particle dispersion in a nonhomogeneous turbulent field, *International Journal of Multiphase Flow* 29, 375–394(2003).

Y.I. Jang, S.J. Lee, “PIV analysis of near wake behind a sphere at a subcritical Reynolds number”, *Experiments in Fluids* 44 (2008) 905-914 (2008).

G.A. Kallio, M.W. Reeks, A numerical simulation of particle deposition in turbulent boundary layers, *International Journal of Multiphase Flow* 3 433-446 (1989).

A. Koster, H. D. Matzner, D. R. Nicholsi, “PBMR design for the future”, *Nuclear Engineering and Design*, 222, 231-245 (2003).

C. Marchioli, M. Picciotto , A. Soldati, Influence of gravity and lift on particle velocity statistics and transfer rates in turbulent vertical channel flow, *International Journal of Multiphase Flow* 33 , 227-251(2007).

Y. Mito, T.J. Hanratty, “Use of a modified Langevin equation to describe turbulent dispersion of fluid particles in a channel flow”. *Flow, Turbulence and Combustion*, 68, 1-26 ((2002).

M.R. Maxey, “The motion of small spherical particles in a cellular flow field”, *Physics of Fluids*, 30, 1915–1928 (1987).

D.J. Thomson, “Criteria for the selection of stochastic models of particle trajectories in turbulent flows”, *Journal of Fluid Mechanics* 180 529-559 (1987).

M. Waldenmaier, “Measurements of inertial Deposition of aerosol particles in regular arrays of spheres”, *J. Aerosol Science* 30, 1281-1290 (1999).